Kirkendall Effect on the Nanoscale

C.Cserháti[1], G.Langer[1], B.Parditka[1], A.Csik[2], Y.Iguchi[2,],Zs.Czigány[3], Z.Erdélyi[1]

[1]University of Debrecen, Department of Solid State Physics, Debrecen, Hungary
[2]Hungarian Academy of Sciences, Institute for Nuclear Research, Debrecen, Hungary
[3]Centre for Energy Research, Institute of Technical Physics and Materials Science

Corresponding author: CsabaCserháti, Department of Solid State Physics, University of Debrecen, 4002 DebrecenP.O.Box 400
e-mail: cserhati.csaba@science.unideb.hu

Abstract

Kirkendall effect has been studied experimentally as well as theoretically for decades already. There are theoretical indications, that the Kirkendall effect must operate from the beginning of the diffusion process but there are practically no measurements on this short time and length scale. For that reason, diffusion on the nanometer scale was investigated experimentally in different binary systems in thin film geometry. We followed the diffusion process as well as the Kirkendall effect by different methods (TEM, SNMS and synchrotron X-ray waveguide technique). Investigations were performed in systems with complete solubility (Bi-Sb, Cu-Ni, Bi-Sb) as well as in systems forming intermetallic phase (Fe-Sb, Fe-Pd). It was found that with these methods the Kirkendall shift can be well followed on the nano-scale. In Fe-Sb system even the bifurcation of the Kirkendall plane was observed.

Keywords

interdiffusion, Kirkendall effect, nano-scale, GIXRF, SNMS

1. Introduction

Since its discovery in 1947, the Kirkendall effect has played an important role in the development of solid state diffusion theory. Kirkendall presented his result of the diffusion experiment of Cu in □-brass. He electroplated a brass bar with Cu, but before he placed inert Mo-wires along each of the two surfaces to mark the original interfaces of the diffusion couple. After heat treatments at 785°C of different times, Kirkendall investigated the cross sections of the diffusion couple and he found that the Mo-wires shifted inwards, moving parabolically with time [1,2,3]. He explained his observation with that the Zn atoms move much faster outwards than the Cu atoms inwards causing the inner brass bar to shrink. Later it turned out that the manifestation of this effect -which was named after its discoverer as Kirkendall effect-, can be the appearance of diffusion porosity [4], generation of mechanical

stress and the deformation of the whole specimen on the macroscopic scale [5]. Even hollow nano-shell formation was explained by the Kirkendall effect [6,7,8].

The first theoretical description was given by Darken, using independent diffusion fluxes for the different constituents [9]. It was also shown from atomistic point of view, that the interdiffusion accompanied by vacancy mechanism leads to Darken's equations, if it is supposed that local equilibrium of vacancy concentration is assumed [10,11]. Vacancies should be created on one side and annihilated on the other side of the diffusion couple for the Kirkendall effect to occur. Following Darken's approach in and A-B binary diffusion couple the marker velocity depends on the difference in intrinsic diffusivities of the two species and the concentration gradient developing in the diffusion zone at the marker plane composition [4,12,13,14]:

$$v = -V_B(D_A - D_B)\frac{\partial C_B}{\partial x}, \tag{1}$$

where v is the velocity of the marker plane positioned initially at the original interface,$V_B$is the partial molar volume of B atoms in $[m^3/mol]$, D_i $[m^2/sec]$ are the diffusion coefficients, C_B $[mol/m^3]$ is the concentration of the B component and x $[m]$ is the position. In this calculation it is always supposed that only volume diffusion takes place. If this is the case, the inert markers positioned at the original interface between the reactants are the only markers that stay at constant composition and moves parabolically in time ($x^2 \propto t, x \propto \sqrt{t}$) during the whole diffusion process. The velocity of the markers than:

$$v_k = \frac{dx}{dt} = \frac{x_k}{2t}, \tag{2}$$

where x_k is the position of the Kirkendall plane.The location of the Kirkendall plane can then be found graphically as the intersection of the marker velocity plot and the straight line given by Eq.(2)if the position of the marker plane is known at the beginning of the diffusion process [15]. If there is no molar volume change during the process, it can be found by the traditional Boltzmann-Matano method [12]. There are several examples in the literature where Kirkendall effect was studied on the micrometer scale. There are binary systems where more than one [16,17], or no Kirkendall plane exist [18].

The motivation of this study was to investigate the Kirkendall effect on a much shorter length scale, namely on the nano-scale, which implies the study of the very beginning of the diffusion process. In order to do this, one need to gain direct information from the composition profile of the diffusion atoms, as well as the position of the inert markers on a short length-scale.

2. Methods and Materials

2.1. Grazing incidence X-ray fluorescence analysis (GIXRF)

The first experimental method we used is the GIXRF with X-ray standing wave technique. The investigated diffusion couple was prepared as thin films placed into a waveguide structure formed by two high atomic number films (W in this case), which acts as a mirror at grazing incidence angle **Figure 1.**a. Thanks to this structure, X-ray standing wave could be generated between the W mirrors because of the total reflection from the W-waveguides. The reflected beam interfering with itself at certain incidence beam angles, the electric field forms a standing wave-like pattern. The condition of this resonance is:

$$\Theta_m = \frac{(m+1)\pi}{kd}, \tag{3}$$

where k is the absolute value of the X-ray wave vector, d is the thickness of the cavity (the distance between the mirror layers). Under this condition, the m'th transverse electric mode (TE) of the waveguide is excited, which propagates undisturbed along its length. **Figure 1.** illustrates the scheme of this electric field. The fluorescence signal from the buried layer originates from the volume where the electric field intensity and the atomic density of the element of interest are overlapping.

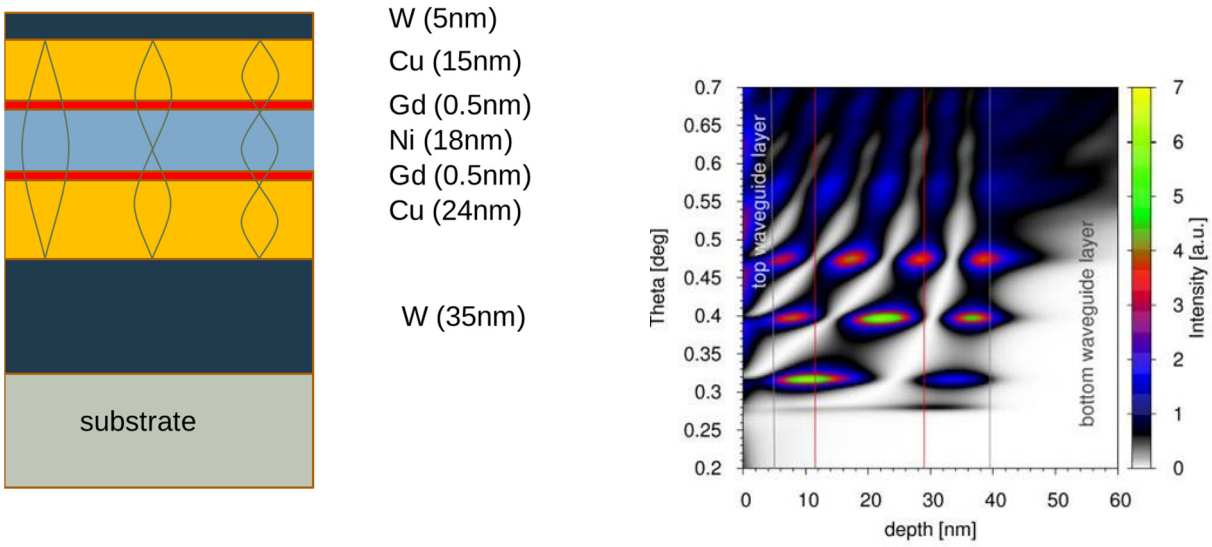

(a) (b)

Figure 1. (a) Waveguide sample structure we have developed and investigated. The W layers are the reflectors, Si is the substrate; the Cu/Ni/Cu tri-layer with Gd markers in between is the 'sample to be investigated. The schemes of the first three TE are also illustrated. (b) Intensity plot of the calculated electric field (photon energy: 7.3keV). The different TE as a function of the incident angle is displayed.

As it is shown on **Figure 1.**, thin Gd layers were used as inert Kirkendall markers. The energy of the X-ray beam was adjusted in a way, that only Gd atoms were excited (E_{beam}=7.3keV). Using a simple approach of Parrat [19], knowing the structure of the sample, the electric field generated between the mirror layers as well as the fluorescence intensity can be calculated according to the following formula [20,21]:

$$I(\Theta) = \int_0^L c(x)E^2(\Theta, x)dx, \tag{4}$$

where c is the atomic fraction of the material which we are interested in, in our case Gd, E is the amplitude of the electric field, L is the length of the sample – including the waveguide layers, and is the incident angle. Changing the incident angle, the electric field (the modus of the standing wave pattern) also changes, i.e. the position of the previously described overlapped zone, as well as the fluorescence intensity varies with changing incident angle **Figure 2**.

If we understand well the structure of the specimen and follow the method given by Parrat [19], applying Eq.(4)it is possible to calculate the fluorescence intensity as a function of the incident angle. By iterative fitting of the measured and simulated intensities, the composition profile of all the constituents can be reconstructed [22,23].

The measurements had been performed at the KMC2 beamline at the BESSY II-Helmholz –Zentrum Berlin (HZB) synchrotron light source. The geometry and the details of the measurement are written elsewhere [23]. Activation energy above the K absorption edge of Gd (7.3keV) was used. Knowing the distribution of Gd in the sample, the incident angle was tuned to produce standing wave patterns with maximal electric field in specific positions in the sample.

2.2. Secondary Neutral Mass Spectroscopy (SNMS)

Depth profiles were also detected by SNMS (INA-X, SPECS GmbH, Berlin). The instrument works with Ar-plasma and the bombarding ion current has an extremely high lateral homogeneity. The low bombarding energies (in order of 10^2eV) and the homogeneous plasma profile result in an outstanding depth resolution (<2 nm) [24]. In these circumstances the detection limit of the machine can be about 10ppm. Details of quantification procedure of SNMS spectra are described in [25,26]. SNMS measurements had been planned and performed on binary thin film systems applying W markers in between to study the Kirkendall effect.

2.3.Sample preparation

A SiO_2(substrate) / W(35nm) / Cu(24nm) / Gd(0.5nm) / Ni(18nm) / Gd(0.5nm) / Cu(15nm) / W(5nm) samples were prepared by magnetron sputtering for synchrotron measurements. SiO_2(substrate)/ Me_1/ W(0.5nm) / Me_2type diffusion couples were prepared as well for SNMS measurements only using the same method. Systems forming solid solution (Cu-Ni, Bi-Sb) and intermetallic phases (Fe-Pd, Fe-Sb) were investigated with both possible packing orders. Note that the Gd layer was prepared by electron beam evaporation.

All the layers were polycrystalline. The films were deposited by magnetron sputtering onto a <111> oriented Si wafers with native SiO_2 layer at the top. The substrates were cleaned and dried as usual just before placed into the evaporation chamber. The parameters of magnetron sputtering were as follows: Ar purity: 99.999%, base vacuum: $p_{base}=5\times10^{-7}$mbar and sputtering Ar pressure: $p_{sput}\approx5\times10^{-3}$mbar.The Gd as well as the W are inert in the diffusion couples we investigated. Since the thicknesses of these films are ~0.5nm they do not form a complete layer between the diffusing constituents but islands. This was confirmed by Atomic Force Microscope (AFM) imaging. The structure of the as deposited samples was checked by Transmission Electron Microscope (TEM), AFM and Secondary Neutral Mass Spectrometry (SNMS).). TEM cross sections were prepaired by FIB technique and investgated in a JEOL3010 electron microscope operated at 300kV.

3. Results and Discussion

3.1. GIXRF

Points on **Figure 2** show a typical fluorescence intensity curve, the line represents the fitted curve, calculated from the supposed sample structure (**Figure 1**) using Eq.(4). The peaks on the curve are due to the overlap of the generated electric field and the Gd atoms, since the energy of the X-ray was tuned to excite only those atoms (E=7.3keV).

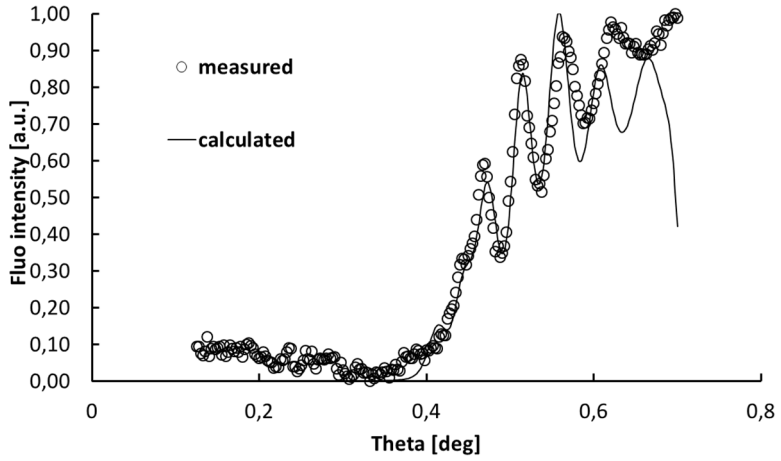

Figure 2. Fluorescence intensity (normalized to one) versus incident angle measured and calculated from Eq. (4); as prepares sample.

The calculated curve fits very well the measurement for low incident angles. At higher angles however, the uniformity of the layer thickness starts to play an important role. Since in real samples, produced by magnetron sputtering, thickness in millimeter range (including the substrate) can vary few nanometers, the signal gets smeared. This effect should not be confused with interface roughness, which was included in calculation. Applying the same method for all the annealed specimens (T=350°C)), the position of the Gd layers can be detected in the samples. **Figure 3** displays that both marker planes moved to the direction of Cu due to the annealing, which was expected because of diffusion data [27]. The marker shift is plotted as a function of $t^{1/2}$, where t is the annealing time.

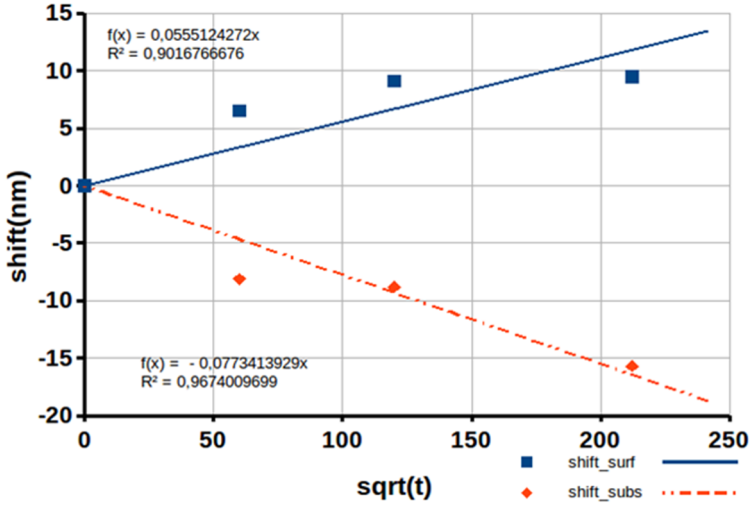

Figure 3. The marker shift is plotted as a function of $t^{1/2}$, where t is the annealing time. The rhombuses show the shift of the Gd markers at K1, while the squares represent the movement of the Kirkendall plane at K2. The annealing temperature was 350°C.

The rhombuses show the shift of the Gd markers close to the surface (K1), while the squares represent the movement of the near-substrate Kirkendall plane (K2). The plot shows, that the relative position of the bottom Gd layer (K2), can be well fitted with a straight line, which indicates that the shift of this Kirkendall plane and the annealing time are related

through a parabolic function. On the other hand, the marker plane which corresponds to the first Cu/Ni interface from the surface (K1), can't be fitted with a line (see **Figure 3**). This indicates that the diffusion process is much faster there.

The difference can be explained by taking into account the segregation tendency of Cu. It is documented before, that the layer sequence during the sample preparation influences the kinetics of the diffusion process, or in some cases the final, equilibrium state as well [28]. In case of the K2 Cu/Ni interface, Ni atoms were deposited on the Cu film. Since Cu has smaller surface energy (i.e. smaller surface tension) than Ni, it tends to segregate on the Ni surface even during the deposition. This results a mixed, diffuse interface between these metallic films at K2. On the other hand, sputtering of Cu onto the Ni layer, see K1 the transition, results a sharp concentration profile at interface K1. Because the diffusion of Ni depends strongly on the nickel concentration, the time dependence of the diffusion process is different on the different interfaces. This phenomenon is called as dynamic segregation and it is accounted for these effects in thin film technology [28]. According to literature data [29,30] the self-diffusion coefficients of both elements in Ni is about four order of magnitude smaller than in Cu at 1000K.

Thus the kinetics of the diffusion process is different at the different interfaces, since the concentration profiles and so the concentration dependence of the self-diffusion coefficients is different. At K1, there is a sharp step on the profile, through the interface. Accordingly there is a sharp step on the self-diffusion coefficient, which results a big change in the diffusion flux of Cu. At K2, the profile is not as sharp as at K1, and the change of the diffusion coefficient, as well as in the diffusion flux of Cu is smoother, which explains the parabolic time dependence of the marker shift at K2 and a different, faster kinetics at K1.

3.2. SNMS

SNMS measurements were also planned and performed to support experiments showing that Kirkendall effect can be measured and even followed on nano-scale. Samples were prepared as it is written above, with the difference, that in these measurements W was used as inert marker in the interdiffusion experiments.

Two different kind of binary systems were investigated. Cu260nm/Ni110nm and Sb300nm/Bi300nm with an almost symmetric miscibility gap and Fe60nm/Pd35nm and Fe75nm/Sb80nm which are phase forming metallic systems. In the INA-X type SNMS extremely plane bombarding craters are obtained when the bombarding voltage (typically few hundred electron volts), the plasma parameters and plasma sample distance are chosen appropriately. As a result, high depth resolution of the order of 1−2 nm can be achieved and maintained over few hundred nm sputtered depth. The raw data provided by the SNMS measurements give us the information with intensity-time profiles. The SNMS intensity versus sputtering time curves of an annealed sample are presented inFigure 4. The determination of the positions of the marker-plane was carried out in subsequent steps. First the curves shown in Figure 4 were determined and the intensity level, I_{max} , belonging to the maximum in the W-intensity was read out. Next the depth of the crater was measured by a profilometer (Amibios XP-I) and in some cases by white light interferometry method as well. This was followed by another etching until the value of I_{max} , belonging to the W-plane in question, was reached and the depth was measured again. In determining the interface position, in each case a new crater was created up to the given W composition. From the depth measurements the shift W can be calculated. The initial position $x_o$was determined on the as-deposited sample. In these measurements only the extent and the direction of the Kirkendall shift was determined.

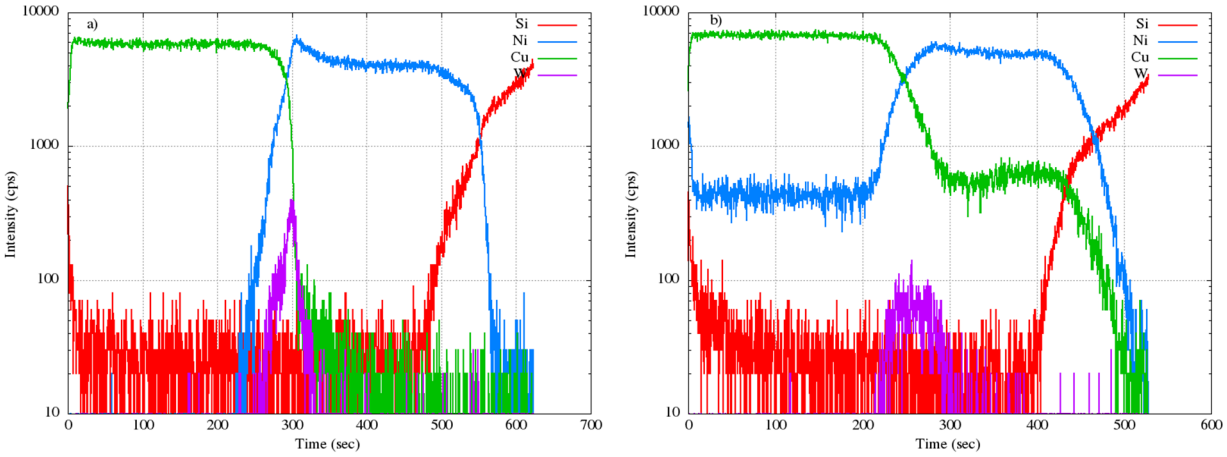

Figure 4. (a) shows the SNMS profile of the as deposited Ni/Cu sample, and (b) displays the SNMS profile of the specimen, which was annealed at 500ºC for 4h. W markers moved into the direction of Cu. Note that W peak is about two times wider. This is the consequence of the slight W dissolution into the Ni.

Figure 4.a shows the SNMS profile of the as deposited Ni/Cu sample and Figure 4.b the profile of the annealed (500ºC, 4h) specimen. Both depth measurements demonstrate that the W markers moved into the direction of Cu with about 40nm±5%. Note that according to these measurements the total thickness of the film decreased by about 8%. This is the result of the compaction as well as the recrystallization of the thin film. On Figure 4.b it is also visible, that the W peak is about two times wider than before. This could be the reason of the fact, that according to literature [31], there is a slight solubility of W in Ni. The concentrations, which can be calculated from the raw data are in correspondence with the binary phase diagram of the system.

Similar measurements were performed on Bi-Sb system with two possible packing order. In one case Bi on the other case Sb was on the top of the film. In the first case, after annealing (250ºC 2h), Kirkendall markers moved into the Bi direction by about 60nm±5%, indicating that this constituent is the faster one. Noted, that interface roughening was observed by bare eye after annealing. The total thickness of the film decreased by about 4% for the same reason.

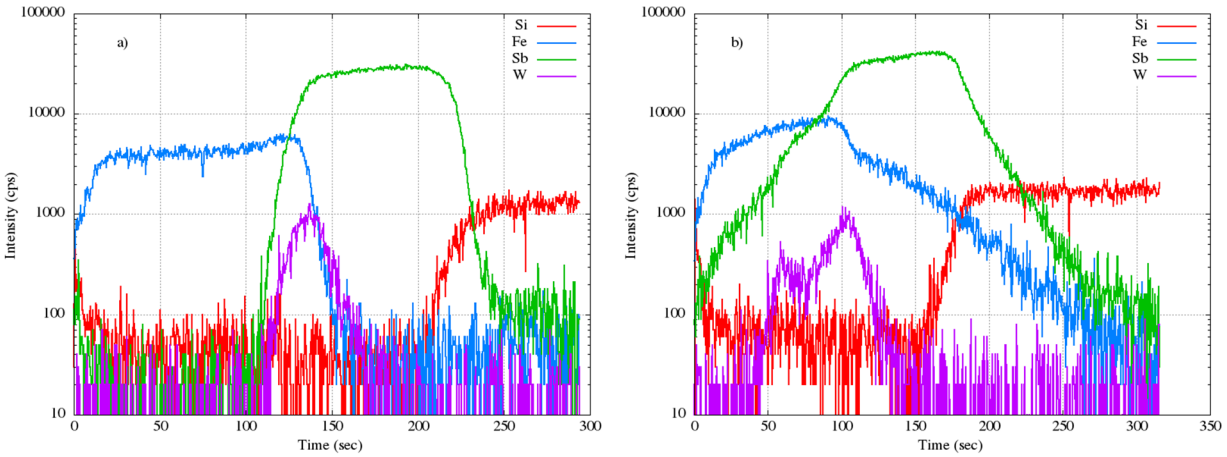

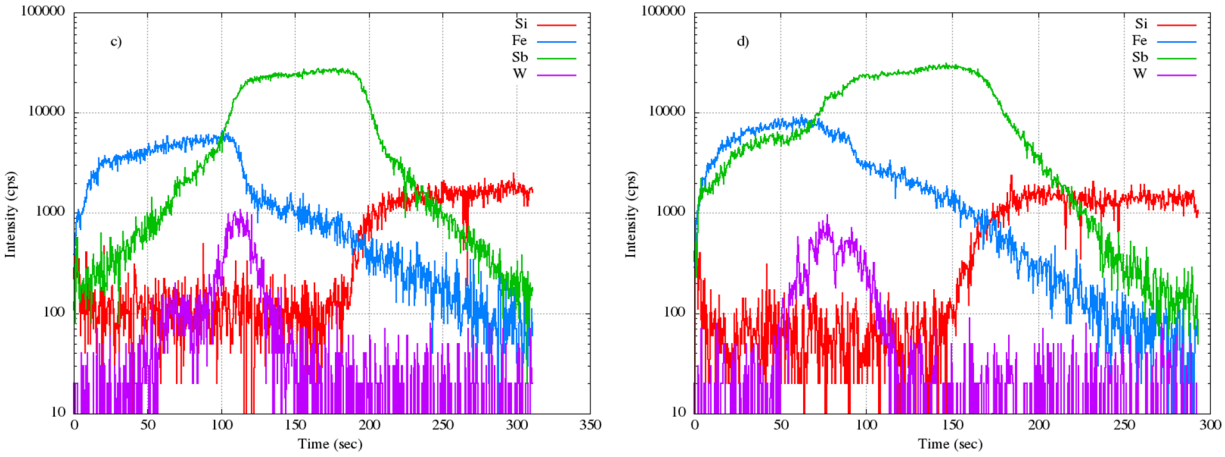

Figure 5. SNMS profiles of Fe-Sb annealed at 350ºC. (a) is the profile of the as deposited sample. After 90min annealing (b), the W peak bifurcates. For further annealing (c) 105 min the peak closer to the surface becomes smaller and after 120 min (d) only one marker-plane is visible.

On the other hand, investigating the other type of sample i.e. Sb was on the top, a different phenomenon occurred. During exactly the same annealing circumstances, W-marker-plane moved into the Sb direction (45nm±5%), although Bi is the faster component in the system. The compositions are again in correspondence with the binary phase diagram of the system.

In the phase forming Fe-Pd the markers shifted by about 20nm into the Fe direction after annealing (400ºC, 1h), indicating that Fe is the fastest component. On one side of the marker plane FePd phase, on the other side pure Fe was observed after annealing. Note, that in this case a concave crater profile was measured.

Studying the Fe-Sb system, unexpected phenomenon occurred (see Figure 5). First of all, as in all the other investigated binary systems the total thickness of the film decreased after annealing by about 3%. Second, when Sb layer was on the top, no diffusion occurred during the annealing but the W profile became a bit wider. On the other hand, when Fe was deposited on the top of Sb, as a result of the annealing (350ºC, 1.5h), the W-markers moved into the Fe direction, as well as divided into two distinct peaks (Figure 5.b). After further annealing of 15min, the W-peak closer to the surface decreased, while the other peak close to the interface increased (Figure 5.c). After 2h of annealing only one W-peak was visible (Figure 5.d). The experiment was repeated several times with the same result.

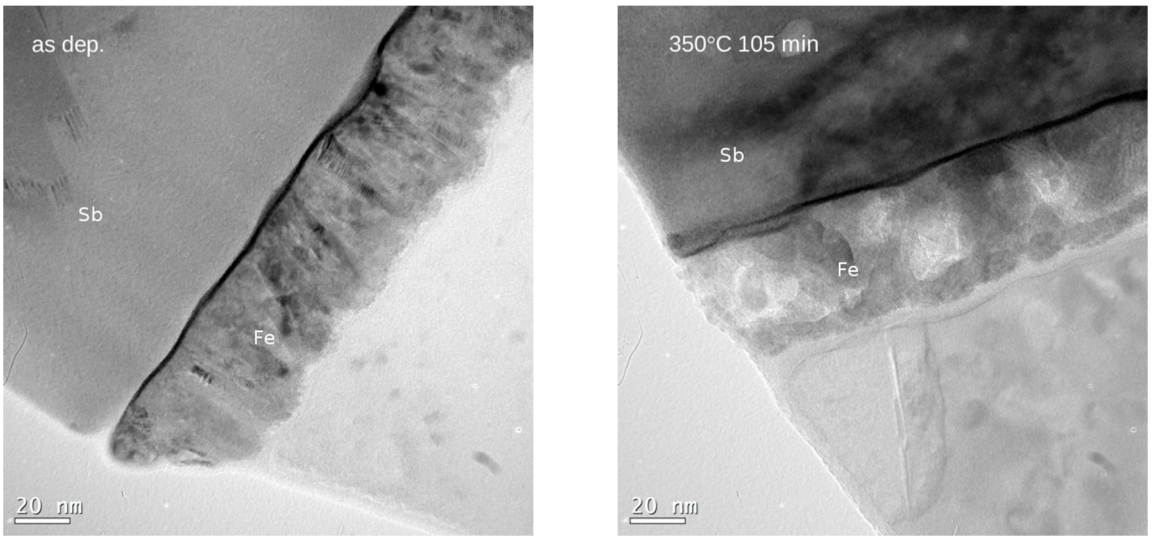

Figure 6. Cross sectional transmission electron microscope images of Fe-Sb sample. (a) shows the as deposited state. Next to the columnar Fe structure the black line indicates the W marker-plane. (b) displays the bifurcated W-plane after annealing at 350°C for 105 min.

For direct monitoring of this phenomenon, cross sectional transmission electron microscope (X-TEM) studies were performed. The specimens were prepared by Focused Ion Beam and investigated with TEM. Figure 6. shows the TEM image of the as deposited as well as the annealed sample. It can be seen, that after annealing, the originally fine columnar structured Fe layer changed into a polycrystalline layer with much bigger grain size. Figure 6.a shows that the W-marker-plane as a black line in between the Fe and Sb layers. Figure 6.b displays that the W layer has changed, it is more wavy than before and in some places it is visibly decomposed into two, which explains the measured SNMS profile.

5. Conclusions

In the present paper we demonstrate, that Kirkendall effect occurs and can be measured on the nano-scale in thin film geometry. We also present the limits of the methods we applied. The difficulties mainly come from the fact that there are different growth mechanisms of thin films [32]. Based on the structure of the developing film, we can distinguish amorphous, polycrystalline, mosaic structures as well as islands forming films. Dynamic segregation can also influence this mechanism [28]. In addition, structural changes in nano-scale during heat treatment have a strong influence on the kinetics of mutual diffusion and on the equilibrium state, such as on the Kikendall effect.

We applied two fundamentally different methods to demonstrate that. First the GIXRF technique was described and applied to follow the Kirkendall-marker-shift in the Cu-Ni system. Special sample structure was used in order to be able to apply the X-ray standing wave technique. The methods allow us to determine the position of the inert Gd-markers which appoint the Kirkendall plane in the interdiffusion process. Using different annealing time, we could follow the kinetics of the process at 350°C. It turned out, that the time evolution depends on the packing sequence of the films. Since Cu always tends to segregate on the Ni surface, two different interface develops during the sample preparation, i.e. the concentration profiles and so the concentration dependence of the self-diffusion coefficients of the two diffusing elements are different. At K1, there is a sharp step on the profile, accordingly there is a sharp step on the self-diffusion coefficient, which results a big change in the diffusion flux of Cu. On the other hand at K2, the profile is smoother and the change of the diffusion coefficient and the diffusion flux of Cu is also lighter. In this way we could explain the parabolic time dependence of the marker shift at K2 and a different, faster marker movement at K1.

It was also demonstrated, that the SNMS method can be used as well to detect the Kirkendall effect. In these measurements W was used to indicate the Kirkendall plane. Four different systems were investigated. In case of Cu-Ni system we demonstrated that during the interdiffusion process, shift of the markers occurs. The measurements with this method also confirm that the packing order influences the process. Studying the Bi-Sb system, the marker-plane always moved into the direction of the free surface independently of the layering sequence. (We have not found any explanation for that.) We have to note that according to our observations, Bi forms islands during deposition on the SiO_2 substrate. We deposited a thin W layer on these islands before the Sb layer. It is very well possible that the growth and recrystallization of these islands influences the diffusion process and so the shift of the marker-plane.

Investigating phase forming binary systems, the occurrence of the Kirkendall effect was proven in Fe-Pd and in Fe-Sb binary metallic systems. Moreover in Fe-Sb, the originally

single W-plane split into two. This observation was also confirmed by X-TEM imaging (Figure 6). On one side of the Kirkendall plane FeSb, while on the other side $FeSb_2$ phase grow. Although there are no diffusion data of the constituents in these phases, the effect can be explained based on publications on the reconsideration of the Kirkendall effect [33,34]. Supposing a Kirkendall velocity curve like in case of Co-Si [35] or in Ni-Ti [36], the bifurcation of the marker plane can be explained. In order to prove this unambiguously, further experiments need to be done to determine the integrated diffusion coefficients [37] of the intermetallic phases in Fe-Sb system.

Acknowledgements

The work was supported by the GINOP 2.3.2-15-2016-00041 (co-financed by the European Union and the European Regional Development Fund) and the EXMONAN EU FP7 project. Y. Iguchi acknowledges Postdoctoral Fellowship Program of the Hungarian Academy of Sciences.

References

[1] A.D. Smigelskas and E.O. Kirkendall, *Trans. AIME* **171,** 130 (1947)
[2] E. Kirkendall, L. Thomassen, C. Upthegrove, *Trans. AIME* **133,** 186–203 (1939)
[3] E. O. Kirkendall, *Trans. AIME* **14 7**104-110 (1942)
[4] Y. A. Geguzin, M. A. Krivoglaz, *Nauka* (in russian) 215 (1979)
[5] I.Daruka, I. A. Szabó, D. L. Beke, C. Cserhati, A. A. Kodentsov, F. J. J. van Loo, *Acta. Mater*. **44** 4981–4993 (1996)
[6] A. M. Gusak, T. V. Zaporozhets, K. N. Tu, U. Gösele, *Philos. Mag*. **85** (36) (2005) 4445–4464.
[7] G. E. Murch, A. V. Evteev, E. V. Levtheko, I. V. Belova, *Diff. Fund.* **42**1–22 (2009)
[8] C. Cserhati, G. Glodán, D. L. Beke, *Diff. Fund.* **1** 61–73 (2014)
[9] L. S. Darken, *Trans. AIME* **175** 184–201 (1948).
[10] F. Seitz, *Phys. Rev.* **74**1513–1523 (1948)
[11] J. Bardeen, Diffusion in Binary Alloys, *Phys. Rev.* **76** 1403–1405 (1949)
[12] J. Philibert: *Atom Movements, Diffusion and Mass Transport in Solids*, Les Editions de Physique, Les Ulis, France, (1991)
[13] J.-F. Cornet and D. Calais: *J. Phys. Chem. Solids* **33** , 1675 (1972)
[14] F. J. J. van Loo: *Prog. Solid State Chem.* **20** , 47 (1990)
[15] M. J. H. van Dal, A. M. Gusak, C. Cserhati, A. A. Kodentsov, and F. J. J. van Loo: *Phys. Rev. Lett.* **86**, 3352-3355 (2001)
[16] M. J. H. van Dal, M. C. L. P. Pleumeekers, A. A. Kodentsov and F. J. J. van Loo: *Acta Mater.* **48** 385-396 (2000)
[17]A. Paul et al.: *Acta Materialia* **52** 623–630 (2004)
[18] M. J. H. van Dal, A. M. Gusak, C. Cserhati, A. A. Kodentsov and F. J. J. van Loo: *Phil. Mag. A* **82**,943 (2002)
[19]L. G. Parratt: *Phys. Rev.* **95**, 359 (1954)
[20]D. L. Windt: *Comput.Phys.* **12**, 360. (1998)
[21] S. K. Ghose, B. N. Dev: *Phys Rev B* **63**, 245409 (2001)
[22] A. Gupta, C. Meneghini, A. Saraiya, G. Principi, D. K. Avasthi: *Nucl. Instrum. Methods. Phys. Res. B* **212**, 458 (2003)
[23] Z. Erdélyi, C. Cserhati, A. Csik, L. Daróczi, G. A. Langer, Z. Balogh, M. Varga, D. L. Beke, I. Zizak and A. Erko: *X-Ray Spectrom.* **38**, 338–342 (2009)
[24] H. Oechsner: *Nucl Instr. Methods PhysRes;B* **33**:918–25 (1988)

[25] K.H. Muller, H. Oechsner: MikrochimActa (Wien) Suppl;**10**:51–60 (1983)
[26] H. Oechsner, R. Getto, M. Kopnarski: *J Appl. Phys* ;063523:105 (2009)
[27]Diffusion In Solids Metals and Alloys; ed. by H. Mehrer, *Landolt-Börnstein, New Series* **III/26** (1990)
[28] S. Labat, P. Gerguad, O. Thomas, B. Gilles, A. Marty: *Appl. Phys. Lett.;***75**:914-916 (1999)
[29] W.F. Egelhoff: *J. Vac. Sci. Technol. A* **7** (3) 2060 (1989)
[30] Z. Erdélyi et al.: *Surface Science* **496** 129-140 (2002)
[31] W. J. Muster, D. N. Yoon, W.J. Huppmann: *Journal of the Less-Common Metals*, **65** 211 – 216 (1979)
[32] *Handbook of Thin Film Process Technology* ed. by: David A Glocker and S Ismat Shah, IOP Publishing Ltd 1995 Bristol and Philadelphia
[33]M.J.H. van Dal, A.M. Gusak, C. Cserhati, A.A. Kodentsov and F.J.J. van Loo, *Phys. Rev. Lett.* **86** 3352 (2001)
[34] A. A. Kodentsov , A. Paul, M. J. H. van Dal, C. Cserhati, A. M. Gusak, F. J. J. van Loo, *Critical Reviews in Solid State and Materials Sciences,* **33**, pp. 210–233, (2008)
[35] M.J.H. van Dal, A.A. Kodentsov and F.J.J. van Loo, *Intermetallics* **9**, 451 (2001)
[36] G.F. Bastin: *Diffusie in het systeem Titanium-Nikkel.* Ph.D. thesis, Eindhoven, The Netherlands (in dutch) (1972).
[37] C. Wagner: *Acta Met.* **17**, 99 (1969).